EFFECTS OF SHAFT WARP AND DISK SKEW ON THE SYNCHRONOUS UNBALANCE RESPONSE OF A MULTIMASS ROTOR IN FLUID FILM BEARINGS

D. J. Salamone, Project Engineer

Compressor Division
Allis-Chalmers Corporation
Milwaukee, Wisconsin

and

E. J. Gunter, Professor

Mechanical and Aerospace Engineering Department
University of Virginia
Charlottesville, Virginia

ABSTRACT

The paper deals with the analysis of the synchronous unbalance response of a multi-mass flexible rotor in linearized fluid film bearings including shaft bow and disc skew. The normal proceedure in treating the dynamic unbalance response of a multi-mass rotor is to use the matrix transfer proceedure and to assume that the rotor shaft is undistorted and that the transverse axis of components such as shrunk on disks are perpendicular to the elastic centerline of the shaft.

In the operation of actual turborotors, however, it is often possible that the idealized shaft and disc assumptions of straightness are violated due to such factors as thermal bowing, excessive loading and improper shrink fits of impeller wheels. In this case, then shaft warp and disc skew introduce effective unbalance forces and moments which can cause large amplitudes of rotor motion when operating in the vicinity of a critical speed.

To illustrate the importance of including disk skew and shaft warp in the dynamical equations, several synchronous response cases are presented, including the evaluation of a large industrial motor driven water pump.

NOMENCLATURE

$A = S_{xx} + S_{px} - m_p\omega^2$

$A_{11} = \dfrac{BS_{xx} - S_{yx}S_{yy}}{Q3}$

$A_{12} = \dfrac{BS_{xy} - S_{xy}S_{yy}}{Q3}$

$A_{21} = \dfrac{-S_{yx}S_{xx} + AS_{yx}}{Q3}$

$A_{22} = \dfrac{-S_{yx}S_{xy} + AS_{yy}}{Q3}$

B	$= S_{yy} + S_{py} - m_p\omega^2$	
c_{px}, c_{py}	Linear pedestal damping	FTL^{-1}
c_{xx}, c_{xy}, c_{yx}, c_{yy}	Linear bearing oil film damping	FTL^{-1}
E	Young's modulus of shaft section	FL^{-2}
I	Area moment of inertia of shaft section	L^4
I_p	Polar mass moment of inertia of disk	FT^2L
I_T	Transverse mass moment of inertia of disk	FT^2L
j	$= \sqrt{-1}$	
k_{px}, k_{py}	Linear pedestal stiffness	FL^{-1}
k_{xx}, k_{xy}, k_{yx}, k_{yy}	Linear bearing oil film stiffness	FL^{-1}
ℓ	Length of rotor shaft section*	L
m_p	Pedestal mass	FT^2L^{-1}
m_s	Total rotor station lumped mass	FT^2L^{-1}
$Q3$	Complex determinant, $= AB - S_{xy}S_{yx}$	-
$\{R\}$	Complex column vector comprising the elements of the ninth column of rows 3, 4, 7 and 8 of the total transfer matrix.	-
S_{px}, S_{py}	Complex pedestal stiffness	FL^{-1}
S_{xx}, S_{xy}, S_{yx}, S_{yy}	Complex bearing oil film stiffness	FL^{-1}
$\{Tc\}$	Complex combined point and field matrix	-
$\{Tf\}$	Complex field transfer matrix	-
$\{Tp\}$	Complex point transfer matrix	-
$\{Tr\}$	Reduced form of complex total transfer matrix containing the remaining coefficients of rows 3, 4, 7 and 8 after boundary conditions have been applied.	-
U	Complex unbalance, $= U_x + jU_y$	FL
U_x, U_y	Unbalance components in the x- and y-directions.	FL
$\{v\}$	Complex displacement column vector for first station (left end) of rotor	-
V_x, V_y	Complex shear force in the x- and y-directions*	F

x, X	Complex absolute mass station displacement (or shaft deflection) in the x-direction*	L
x_d	Shaft distortion (warp) deflection in the x-direction*	L
y, Y	Complex absolute mass station displacement (or shaft deflection) in the y-direction*	L
y_d	Shaft distortion (warp) deflection in the y-direction*.	L
Z_{bxx}, Z_{bxy}, Z_{byx}, Z_{byy}	Combined bearing and pedestal complex stiffness.	FL^{-1}
γ	$= m_s\omega^2 - Z_{bxx}$	-
$\Delta M_x, \Delta M_y$	Complex skewed disk gyroscopic moments about the y- and x-axes.	FL
$\Delta s_x, \Delta s_y$	Complex distortion (warp) slopes	rad
$\Delta V_x, \Delta V_y$	Complex unbalance driving forces in the x- and y- directions	F
$\Delta w_x, \Delta w_x$	Complex distortion (warp) deflections	L
Δ_x, Δ_y	Net distortion (warp) deflections across the shaft section in the x- and y-directions.	L
$\Delta\theta_x, \Delta\theta_y$	Net distortion (warp) slopes across the shaft section about the y- and minus x-axes	rad
η	$= Z_{byx}$	FL^{-1}
$\theta_x, \tilde{\theta}_x$	Complex shaft slope about the x-axis	rad
$\theta_y, \tilde{\theta}_y$	Complex shaft slope about the minus x-axis (opposite the +y-rotation direction)	rad
$\theta_{x,d}$ $\theta_{y,d}$	Shaft distortion (warp) slopes about the y- and minus x-axes*	rad
λ	$= Z_{bxy}$	FL^{-1}
τ	Complex disk skew, $\tau_x + j\tau_y$	rad
τ_x, τ_y	Permanent disk skew angles about the y-and minus x-axes	rad
α	$= m_s\omega^2 - Z_{byy}$	-
ω	Angular shaft rotational velocity	T^{-1}

*When an i (or i-1) subscript appears on the variables marked with an asterisk, it denotes end i (or end i-1) of rotor shaft section i. An i subscript can also denote mass station i or section i, depending on its context.

INTRODUCTION

Until recently the standard procedure in treating the synchronous unbalance response of a multimass rotor in fluid film bearings has been to assume that the shaft elastic centerline is initially undistorted, and that the transverse axes of all external components (represented mathematically as disks) remain perpendicular to the elastic centerline of the shaft. These two assumptions ignore shaft warp and disk skew excitations, respectively.

Extensive publications are available on the dynamic unbalance response of complex flexible rotor systems by such authors as Lund and Orcutt (1); Kawamo, Matsukura, and Inoue (2); Kirk and Gunter (3); Wolfe and Wong (4); Barrett, Gunter and Allaire (5); and Koenig (6). These investigations have been focused primarily on rotor excitation due to asymmetric radial mass distributions or disk eccentricities. However, rotor shaft warp and disk skew introduce effective unbalance forces and moments that can induce large amplitudes of motion on the rotor when it is operating in the vicinity of critical speeds. Ultimately, these large amplitudes can lead to extensive rotor and bearing damage. As a result, there have been several studies conducted to research these complex effects.

The case of the single-mass rotor on rigid bearings with a warped shaft and radial unbalance has been treated by Nicholas, Gunter, and Allaire (7) at the University of Virginia. This study has provided considerable insight into the behavior of a rotor operating through the first critical speed. However, the results of this work, for the single-mass rotor on rigid bearings, cannot be readily extrapolated to multi-mass rotors on flexible bearings, particularly when these rotors operate through several critical speeds. In addition, their study does not include the effects of disk skew.

For a single-mass rotor system, the incorporation of disk skew is considerably more complicated than the treatment of the warped shaft. In order to examine the influence of disk skew, two additional equations of motion must be considered to represent the disk angular motion and gyroscopic moments. Yamamoto (8) presented the general equations of motion for a skewed disk, transformed into linearized stationary coordinates, with small displacements and rotations. However, the work of Yamamoto does not address the influence of permanent disk skew on shaft dynamics.

The case of a single, overhung skewed disk on an undistorted, uniform elastic shaft was treated by Benson (9) at the University of Virginia. Benson demonstrated that permanent disk skew can have a pronounced effect on the dynamics of the rotor shaft and that the single-plane balancing procedure is not adequate to balance the overhung skewed disk at all speeds. However, this work cannot be directly applied to multi-mass rotors and it does not include shaft warp.

Kikuchi (10) has formulated the matrix transfer equations for the unbalance response of a multi-mass flexible rotor with shaft distortion, but this work does not consider the permanent disk skew effects. The Kikuchi concept is outstanding in formulating the equations for the general bowed (warped) rotor. However, there are several errors in the algebraic signs and the matrix terms. A comparison of the author's matrix terms and the Kikuchi terms is presented in Reference (11).

This paper includes the effects of disk skew and shaft warp, in addition to the commonly treated unbalance excitation, for synchronous rotor response. The numerical results were calculated on a digital computer program which implements the dynamic transfer matrix equations for a general multi-mass flexible rotor in fluid film bearings. All eight bearing stiffness and damping coefficients are considered.

To illustrate the importance of including disk skew and shaft warp in these dynamic equations, several synchronous response cases are presented for a large industrial water pump, in which the bearing damping was reduced by a factor of

20 from the original values to excite the first three critical speeds. For the five cases considered, shaft warp was the dominant excitation at the first critical speed, shaft warp and disk skew were dominant at the second critical speed, and the disk skew dominated the third critical speed. For all three critical speeds, the predominant excitation was not unbalance. Hence, a synchronous response analysis that only considers unbalance excitation would be greatly in error if the actual machine has skewed disks or a warped shaft (including coupling misalignment). This error is particularly significant at the rotor critical speeds, which in many machines are excited without reducing the bearing damping. Due to the limitations of manufacturing tolerances, these excitations will always exist to some degree and their influence on rotor behavior must be assessed.

TRANSFER MATRIX FORMULATION

The equations of motion, represented in transfer matrix form, mathematically consider a lumped mass rotor model, consisting of a series of lumped masses connected by a massless elastic shaft. These equations are applicable only to elastic force-displacement relations. The rotor shaft may be supported by speed-dependent, damped, asymmetric bearings in flexible damped pedestals. All eight bearing stiffness and damping coefficients are considered.

The derived transfer matrix includes the equations of motion for the response of a rotor with unbalanced masses, permanently skewed disks, and a warped shaft. An unbalanced mass is created when the geometric center of an external rotor component (represented mathematically as a disk) is eccentric to its mass center by some distance, e_u. A disk is permanently skewed when its transverse axis is not perpendicular to the elastic centerline of the shaft. Shaft warp results when the elastic centerline of the rotor shaft is distorted. Note that the term "warp" used in this paper differs from the warp in classical engineering mechanics. The latter means that plane sections do not remain plane.

The total transfer matrix for a given shaft section is composed of the combined properties of the point matrix which includes all of the shaft inertia properties, unbalance and disk skew which are concentrated at a point and the field transfer matrix which includes shaft warpage. Fig. 1 represents a typical rotor mass station with shear transfer from the adjacent shaft sections and bearing forces. In addition to bearing forces, the pedestal or foundation motion may also be incorporated in the point matrix.

A typical shaft elastic station including shaft warp is shown in Fig. 2 for the Y-Z plane. A similar figure can also be presented for the X-Z plane. Note that in this figure the disc skew angle τ_y is shown in which the disk is skewed a small angle from the shaft elastic centerline.

The point transfer matrix [Tp] across the i-th mass station is of the form

$$\{A\}_i = \begin{Bmatrix} x \\ \theta_x \\ M_x \\ V_x \\ y \\ \theta_y \\ M_y \\ V_y \\ 1 \end{Bmatrix}_i = [Tp] \begin{Bmatrix} x \\ \theta_x \\ M_x \\ V_x \\ y \\ \theta_y \\ M_y \\ V_y \\ 1 \end{Bmatrix}_i = [Tp] \{A\}_i \qquad (1)$$

The field transfer matrix [Tf] across the i-th section is of the form

$$\{A\}_i = \begin{Bmatrix} x \\ \theta_x \\ M_x \\ V_x \\ y \\ \theta_y \\ M_y \\ V_y \\ 1 \end{Bmatrix}_i = [Tf] \begin{Bmatrix} x \\ \theta_x \\ M_x \\ V_x \\ y \\ \theta_y \\ M_y \\ V_y \\ 1 \end{Bmatrix}_{i-1} = [Tf] \{A\}_{i-1} \qquad (2)$$

After substituting the matrix of field equations (2) into the matrix of point equations (1), the "combined point and field transfer matrix" for the i-th section and mass station is obtained.

$$\{A\}_i = [Tp]\,[Tf]\,\{A\}_{i-1} \qquad (3)$$

which can be rewritten in the form

$$\{A\}_i = [Tc]\,\{A\}_{i-1} \qquad (4)$$

This combined matrix [Tc] defines the properties at end i of the i-th mass station in terms of the properties at end (i-1) of the i-th section. Thus, the combined point and field matrix is shown as follows in Table 1, (Equation (5)).

TABLE 1 Combined Point and Field Matrix

$$\begin{Bmatrix} x \\ \theta_x \\ M_x \\ V_x \\ y \\ \theta_y \\ M_y \\ V_y \\ 1 \end{Bmatrix}_i = \left[\begin{array}{cccc:cccc:c} 1 & \ell & \frac{\ell^2}{2EI} & \frac{\ell^3}{6EI} & 0 & 0 & 0 & 0 & \Delta w_x \\ 0 & 1 & \frac{\ell}{EI} & \frac{\ell^2}{2EI} & 0 & 0 & 0 & 0 & \Delta s_x \\ 0 & -\omega^2 I_T & -\omega^2 I_T\frac{\ell}{EI}+1 & -\omega^2 I_T\frac{\ell^2}{2EI}+\ell & 0 & j\omega^2 I_P & j\omega^2 I_P\frac{\ell}{EI} & j\omega^2 I_P\frac{\ell^2}{2EI} & \begin{array}{l}-\omega^2 I_T\Delta s_x \\ +j\omega^2 I_P\Delta s_y \\ +\Delta M_x\end{array} \\ \gamma & \gamma\ell & \gamma\frac{\ell^2}{2EI} & \gamma\frac{\ell^3}{6EI}+1 & -\lambda & -\lambda\ell & -\lambda\frac{\ell^2}{2EI} & -\lambda\frac{\ell^3}{6EI} & \begin{array}{l}\gamma\Delta w_x-\lambda\Delta w_y \\ +\Delta V_x\end{array} \\ \hdashline 0 & 0 & 0 & 0 & 1 & \ell & \frac{\ell^2}{2EI} & \frac{\ell^3}{6EI} & \Delta w_y \\ 0 & 0 & 0 & 0 & 0 & 1 & \frac{\ell}{EI} & \frac{\ell^2}{2EI} & \Delta s_y \\ 0 & -j\omega^2 I_P & -j\omega^2 I_P\frac{\ell}{EI} & -j\omega^2 I_P\frac{\ell^2}{2EI} & 0 & -\omega^2 I_T & -\omega^2 I_T\frac{\ell}{EI}+1 & -\omega^2 I_T\frac{\ell^2}{2EI}+\ell & \begin{array}{l}-j\omega^2 I_P\Delta s_x \\ -\omega^2 I_T\Delta s_y \\ +\Delta M_y\end{array} \\ -\eta & -\eta\ell & -\eta\frac{\ell^2}{2EI} & -\eta\frac{\ell^3}{6EI} & \alpha & \alpha\ell & \alpha\frac{\ell^2}{2EI} & \alpha\frac{\ell^3}{6EI}+1 & \begin{array}{l}-\eta\Delta w_x \\ +\alpha\Delta w_y+\Delta V_y\end{array} \\ \hdashline 0 & 0 & 0 & 0 & 0 & 0 & 0 & 0 & 1 \end{array}\right] \begin{Bmatrix} x \\ \theta_x \\ M_x \\ V_x \\ y \\ \theta_y \\ M_y \\ V_y \\ 1 \end{Bmatrix}_{i-1} \qquad (5)$$

Note: Symbols used here are defined in Appendix A.

This combined transfer matrix $[Tc]_i$ must be formulated for each (i-th) mass station and adjacent shaft section across the entire rotor. The first combined transfer matrix defines the state vector for station 2 in terms of the state vector for station 1.

$$\{A\}_2 = [Tc_1]\ \{A\}_1 \tag{6}$$

The i-th combined transfer matrix (in general) defines the state vector for station i in terms of the state vector for station i-1.

$$\{A\}_i = [Tc_i]\ \{A\}_{i-1} \tag{7}$$

Finally, the n-th (or last) combined matrix defines the state vector for station n (the last rotor station) in terms of the state vector for station (n-1)

$$\{A\}_n = [Tc_n]\ \{A\}_{n-1} \tag{8}$$

After performing the multiplication of the combined transfer matrices, in descending order, the total combined transfer matrix $[Tc]_{total}$ across the entire rotor is obtained. This matrix defines the state vector at the right end of the rotor (station n) in terms of the state vector at the left end of the rotor (station 1). Thus,

$$\begin{Bmatrix} x \\ \theta_x \\ M_x \\ V_x \\ y \\ \theta_y \\ M_y \\ V_y \\ 1 \end{Bmatrix}_n = \left\{ [Tc_n] \cdot \ldots \cdot [Tc_i] \cdot \ldots \cdot [Tc_2] \cdot \ldots \cdot [Tc_1] \right\} \begin{Bmatrix} x \\ \theta_x \\ M_x \\ V_x \\ y \\ \theta_y \\ M_y \\ V_y \\ 1 \end{Bmatrix}_1 \tag{9}$$

Matrix equation (9) is of the general form

$$\{A\}_n = [Tc]_{total}\ \{A\}_1 \tag{10}$$

The boundary conditions at the end of the rotor are free, so that the shears and moments are zero at station 1 and station n. Therefore,

$$M_{x1} = M_{y1} = V_{x1} = V_{y1} = 0 \quad \text{(at left end of rotor)} \tag{11}$$

$$M_{xn} = M_{yn} = V_{xn} = V_{yn} = 0 \quad \text{(at right end of rotor)} \tag{12}$$

After applying the boundary conditions (equations 11 and 12), equation (9) becomes

$$\begin{Bmatrix} x \\ \theta_x \\ 0 \\ 0 \\ y \\ \theta_y \\ 0 \\ 0 \\ 1 \end{Bmatrix}_n = \left[\begin{array}{cccc:cccc:c} t_{11} & t_{12} & t_{13} & t_{14} & t_{15} & t_{16} & t_{17} & t_{18} & t_{19} \\ t_{21} & t_{22} & t_{23} & t_{24} & t_{25} & t_{26} & t_{27} & t_{28} & t_{29} \\ t_{31} & t_{32} & t_{33} & t_{34} & t_{35} & t_{36} & t_{37} & t_{38} & t_{39} \\ t_{41} & t_{42} & t_{43} & t_{44} & t_{45} & t_{46} & t_{47} & t_{48} & t_{49} \\ \hdashline t_{51} & t_{52} & t_{53} & t_{54} & t_{55} & t_{56} & t_{57} & t_{58} & t_{59} \\ t_{61} & t_{62} & t_{63} & t_{64} & t_{65} & t_{66} & t_{67} & t_{68} & t_{69} \\ t_{71} & t_{72} & t_{73} & t_{74} & t_{75} & t_{76} & t_{77} & t_{78} & t_{79} \\ t_{81} & t_{82} & t_{83} & t_{84} & t_{85} & t_{86} & t_{87} & t_{88} & t_{89} \\ \hdashline 0 & 0 & 0 & 0 & 0 & 0 & 0 & 0 & 0 \end{array}\right] \begin{Bmatrix} x \\ \theta_x \\ 0 \\ 0 \\ y \\ \theta_y \\ 0 \\ 0 \\ 1 \end{Bmatrix}_1 \tag{13}$$

Which reduces to

$$\begin{Bmatrix} -t_{39} \\ -t_{49} \\ -t_{79} \\ -t_{89} \end{Bmatrix} = \begin{bmatrix} t_{31} & t_{32} & t_{35} & t_{36} \\ t_{41} & t_{42} & t_{45} & t_{46} \\ t_{71} & t_{72} & t_{75} & t_{76} \\ t_{81} & t_{82} & t_{85} & t_{86} \end{bmatrix} \begin{Bmatrix} x_1 \\ \theta_{x1} \\ y_1 \\ \theta_{y1} \end{Bmatrix} \tag{14}$$

Equation (14) is in the form

$$\{R\} = [Tr]\ \{v\} \tag{15}$$

Where [Tr] is the reduced form of the total combined transfer matrix, [Tc]. Now, solve for {v}, which contains the unknown displacements and slopes at the left end of the rotor. Multiply both sides of equation (15) by $[Tr]^{-1}$, which becomes

$$[Tr]^{-1}\{R\} = [Tr][Tr]^{-1}\{v\} \tag{16}$$

or

$$\{v\} = [Tr]^{-1}\ \{R\} \tag{17}$$

where

$$\{v\} = \begin{bmatrix} x_1 \\ \theta_{x1} \\ y_1 \\ \theta_{y1} \end{bmatrix} \tag{18}$$

Now that the displacements and slopes at the left end of the rotor are known, start at station 1 and apply each combined transfer matrix, equations (6) through (8), in sequence along the rotor to obtain the displacements, slopes, moments, and shears at each adjoining station. Starting with equation (6), use state

vector 1 to solve for unknowns in state vector 2 (where $M_{x_1} = M_{y_1} = V_{x_1} = V_{y_1} = 0$).

$$\begin{Bmatrix} x \\ \theta_x \\ M_x \\ V_x \\ y \\ \theta_y \\ M_y \\ V_y \\ 1 \end{Bmatrix}_{2_{unknown}} = [Tc_1] \begin{Bmatrix} \text{known } x \\ \text{known } \theta_x \\ 0 \\ 0 \\ \text{known } y \\ \text{known } \theta_y \\ 0 \\ 0 \\ 1 \end{Bmatrix}_1 \tag{19}$$

Continue with the general equation (7) to solve for the i-th state vector in terms of the (i-1)-th state vector:

$$\begin{Bmatrix} x \\ \theta_x \\ M_x \\ V_x \\ y \\ \theta_y \\ M_y \\ V_y \\ 1 \end{Bmatrix}_{i_{unknown}} = [Tc_i] \begin{Bmatrix} \text{known } x \\ \text{known } \theta_x \\ \text{known } M_x \\ \text{known } V_x \\ \text{known } y \\ \text{known } \theta_y \\ \text{known } M_y \\ \text{known } V_y \\ 1 \end{Bmatrix}_{i-1} \tag{20}$$

Finally, for the n-th (last) state vector, apply equation (8) (where $M_{xn} = M_{yn} = V_{xn} = V_{yn} = 0$):

$$\begin{Bmatrix} x \\ \theta_x \\ 0 \\ 0 \\ y \\ \theta_y \\ 0 \\ 0 \\ 1 \end{Bmatrix}_{n_{unknown}} = [Tc_n] \begin{Bmatrix} \text{known } x \\ \text{known } \theta_x \\ \text{known } M_x \\ \text{known } V_x \\ \text{known } y \\ \text{known } \theta_y \\ \text{known } M_y \\ \text{known } V_y \\ 1 \end{Bmatrix}_{n-1} \tag{21}$$

Now the complex rotor displacements, slopes, moments, and shears are defined at each discrete mass station along the rotor.

APPLICATIONS - SINGLE MASS ROTOR

In order to verify the accuracy and the validity of the computer program (SYNCWUS) which was designed to calculated the characteristics of a multi-mass rotor system, the program was applied to the well known single mass rotor.

In the first case, a centrally located single mass rotor with a shaft bow of δ_r = 0.125 mils and an unbalance eccentricity of e_u = 0.25 mils as shown in Fig. 3 was calculated. This systen was analyzed in detail in Ref. (7) to determine the influence of various combinations of shaft bow and disk unbalance.

The results of the calculations are shown in Fig. 4 for two values of the dimensionless damping coefficients ζ. As can be seen from the figure, the computer predictions are in excellent agreement with the results presented in Ref. (7).

In the simple Jeffcott model of Fig. 3, the effects of gyroscopic moments and disk skew are not considered. In the second case considered, a single overhung rotor with a skewed disk was examined. The case chosen was similar to the model developed by Benson (9) for the single overhung rotor on a massless elastic shaft as shown in Fig. 5. In this model the disk is skewed by 0.0674° and has a radial unbalance eccentricity of e_u = 10 mils. A comparison between the results generated by the SYNCWUS computer program and the analysis by Benson for the single skewed disk is shown in Fig. 6. Numerous other cases for the single mass rotor were also calculated with excellent agreement between the multimass computer program and the results as predicted by Benson using single mass theory.

The case of the overhung rotor with disk skew and radial unbalance is of considerable interest. The system may exhibit two critical speeds depending upon whether the transverse moment of inertia, I_T is larger than the polar moment of inertia Ip. In this case, it is always possible to select the values of radial unbalance and disc skew such that one of the critical speed modes will be perfectly balanced, but not the other. The implication of this is that it is possible to have an overhung rotor that appears to be in perfect balance at one speed, but is badly out of balance at another speed due to the combined effects of disk skew and radial unbalance. This characteristic and its influence on balancing will be presented in detail in a future paper.

Application - Multimass Motor-Water Pump

To illustrate the practical applications of these dynamic equations, several synchronous response cases are presented for an industrial rotor. The rotor system to be examined is a 45,330 lb. vertical centrifugal water pump consisting of a 40,169 lb motor and a 5,161 lb. pump. The motor is supported by two tilting pad, oil-lubricated bearings and is rigidly coupled to the pump, which is supported by an externally pressurized water-lubricated journal bearing. Figure (7) illustrates the 40-station model for the entire rotor system, indicating the locations of the bearings and the major external rotor components.

The primary sources of rotor excitation in this system are the following:

1. Unbalance and permanent skew at the 11,025 lb. flywheel.
2. Unbalance at the motor core.
3. Angular and parallel coupling misalignment at the motor end flange (forms of shaft warp).
4. Unbalance and permanent skew at the 1,770 lb. impeller.

Note that the impeller imposes hydraulic dynamic unbalance excitation (due to vane imperfections) as well as mechanical unbalance excitation. However, the

hydraulic effects are of primary importance because other magnitudes greatly exceed those due to residual mechanical unbalance.

Case A assumes small residual unbalances of 50 oz-in. each at the flywheel and the motor core. The impeller has a hydraulic dynamic unbalance of 636.78 oz.-in. These unbalances are all in the x-direction (in phase). At the pump operating speed (1190 rpm), this amount of unbalance would produce a load equivalent to a 2.04-lbf weight placed at the outer radius of the impeller (19.5 in.).

Case B also has the same unbalance distribution as Case A. In addition to this unbalance excitation, the flywheel is permanently skewed by an angle τ_x = 0.0058798 degrees (the skew is in phase with the unbalance). The positive skew angle should cause restoring moments on the shaft that would tend to increase the upper motor bearing amplitude from the Case 1 value for this rotor mode. An unbalance couple of 882.0 oz.-in., acting on the flywheel, would produce the equivalent to this amount of skew.

Case C has the same unbalance distribution as in Case A, but the impeller is permanently skewed by an angle τ_x = -0.073048 degrees (the skew is in phase with the unbalance). The negative skew angle should cause restoring moments on the shaft that tend to increase the impeller and water bearing amplitudes for this rotor mode. This particular skew angle produces the equivalent to an unbalance couple of 212.4 oz.-in. acting on the impeller.

Case D considers a $\theta_{x,d}$ = +0.025 degree angular coupling misalignment of the pump shaft at the motor end flange, and the same unbalance distribution as Case A. The misaligned pump shaft lies in a plane that is oriented at the shaft timing mark. Angular coupling misalignment can result when the mating motor or pump flange has not been machined truly perpendicular to the axial centerline of the shaft. When the mating coupling flanges are bolted together, the axial centerlines of the motor and pump shafts are not coincident. Hence, there is a built-in distortion angle between them. This misalignment induces a form of warp (or shaft distortion) excitation on the rotor system.

Case E is a combination run that includes excitation due to unbalanced mass, flywheel skew, impeller skew, and angular coupling misalignment. The unbalance distribution is the same as in Case A, the flywheel has a permanent skew angle τ_x = 0.0058798 degrees, the impeller has a permanent skew angle τ_x = -0.073048 degrees, and the angular coupling misalignment $\theta_{x,d}$ = +0.025 degrees. Note that this is a combination of Cases A, B, C, and D.

To more clearly illustrate the significance of the disk skew and shaft warp effects, the damping in the three bearings was lowered to 1/20 of the original values to excite the first three undamped critical speeds, 484, 2132, and 3012 rpm. The mode shapes corresponding to these critical speeds are illustrated in Figures 8, 9, and 10. Figure 11 is a plot of the resultant pump impeller x-probe amplitudes for these excitation cases (A through E) and Tables 2, 3, and 4 contain tabulations of the rotor amplitudes at six rotor locations for the first, second, and third peak response speeds. This figure illustrates the significant differences between the synchronous pump impeller x-probe amplitudes due to unbalance alone and those due to the addition of shaft warp and disk skew effects, in various combinations with the same unbalance distribution. Note that the angular warp and combination curves do not go to zero amplitude at zero speed, like the unbalance curve. This is because the warp is a permanent shaft distortion. Hence, it produces a low speed runout in shaft amplitude.

The first peak response[1] occurs at 175 rpm for the warp and combination excitations. This peak represents the excitation of the first undamped critical

[1] The rotor speed at which maximum (peak) amplitude occurs. This peak occurs when a critical speed is excited by synchronous driving forces. Note that the undamped rotor critical speeds might not be excited if there is enough damping present in that mode.

Table 2 Rotor First Peak Response Comparison (1/20 Original Damping), x-Probe Peak Amplitudes

Excitation type[a]	Upper motor brg	Fly-wheel	Lower motor brg	Lower cplng flange	Pump water brg	Impel-ler
Case A — Unbalance						
Amplitudes, mils Peak speed, rpm	← First peak not excited →					
Case B — Flywheel Skew						
Amplitudes, mils Peak speed, rpm Change, %[b]	← First peak not excited →					
Case C — Impeller Skew						
Amplitudes, mils Peak speed, rpm Change, %	← First peak not excited →					
Case D — Angular Warp (coupling misalignment)						
Amplitudes, mils	0.69	--	1.65	12.26	39.77	53.58
Peak speed, rpm	(350)	--	(350)	(175)	(175)	(175)
Change, %	--	--	--	--	--	--
Case E — Combination (unbal., warp, skew)						
Amplitudes, mils	0.70	--	1.67	12.27	39.83	53.68
Peak speed, rpm	(350)	--	(350)	(175)	(175)	(175)
Change, %	--	--	--	--	--	--

[a] Specific excitations:

Case A — Flywheel 50 oz.-in.; motor core 50 oz.-in.; impeller 636.78 oz.-in.
Case B — $\tau = 0.0058798°$; unbalance same as for Case A.
Case C — $\tau = -0.073048°$; unbalance same as for Case A.
Case D — $\theta_d = 0.025°$; unbalance same as for Case A.
Case E — Combination of Cases A, B, C, and D.

[b] Change (%) from Case A: + indicates increase; - indicates decrease.

Table 3 Rotor Second Peak Response Comparison (1/20 Original Damping), x-Probe Peak Amplitudes

Excitation type[a]	Upper motor brg	Fly-wheel	Lower motor brg	Lower cplng flange	Pump water brg	Impel-ler
Case A — Unbalance						
Amplitudes, mils	1.76	3.41	3.02	28.41	--	49.39
Peak speed, rpm	(2075)	(2075)	(2100)	(2175)	--	(2175)
Case B — Flywheel Skew						
Amplitudes, mils	5.44	10.19	2.54	27.41	--	47.66
Peak speed, rpm	(2175)	(2200)	(2075)	(2200)	--	(2175)
Change, %[b]	+209.1	+198.8	-15.9	-3.5	--	-3.5
Case C — Impeller Skew						
Amplitudes, mils	1.66	3.11	2.86	32.98	--	57.21
Peak speed, rpm	(2075)	(2075)	(2075)	(2175)	--	(2175)
Change, %	-5.7	-8.8	-5.3	+16.1	--	+15.8
Case D — Angular Warp (coupling misalignment)						
Amplitudes, mils	12.21	11.23	6.54	32.40	10.47	51.22
Peak speed, rpm	(2200)	(2075)	(2100)	(2175)	(2100)	(2175)
Change, %	+593.8	+229.3	+116.6	+14.0	--	+3.7
Case E — Combination (unbal., warp, skew)						
Amplitudes, mils	4.33	8.36	5.21	35.56	11.99	57.22
Peak speed, rpm	(2075)	(2075)	(2100)	(2175)	(2125)	(2175)
Change, %	+146.0	+145.2	+72.5	+25.2	--	+15.9

[a] Specific excitations:

Case A -- Flywheel 50 oz.-in.; motor core 50 oz.-in.; impeller 636.78 oz.-in.
Case B -- $\tau = 0.0058798°$; unbalance same as for Case A.
Case C -- $\tau = -0.073048°$; unbalance same as for Case A.
Case D -- $\theta_d = 0.025°$; unbalance same as for Case A.
Case E -- Combination of Cases A, B, C, and D.

[b] Change from Case A (%): + indicates increase; - indicates decrease.

Table 4 Rotor Third Peak Response Comparison (1/20 Original Damping), x-Probe Peak Amplitudes

Excitation type[a]	Upper motor brg	Fly-wheel	Lower motor brg	Lower cplng flange	Pump water brg	Impel-ler
Case A — Unbalance						
Amplitudes, mils	1.36	1.57	6.58	47.08	18.39	82.03
Peak speed, rpm	(2650)	(2675)	(2525)	(2550)	(2475)	(2550)
Case B — Flywheel Skew						
Amplitudes, mils	1.17	1.28	6.61	47.28	18.47	82.29
Peak speed, rpm	(2600)	(2650)	(2550)	(2550)	(2475)	(2550)
Change, %[b]	-14.0	-18.5	+0.5	+0.4	+0.4	+0.3
Case C — Impeller Skew						
Amplitudes, mils	1.56	1.77	7.81	55.83	21.69	95.80
Peak speed, rpm	(2650)	(2675)	(2550)	(2550)	(2475)	(2550)
Change, %	+14.7	+12.7	+18.7	+18.6	+17.9	+16.8
Case D — Angular Warp (coupling misalignment)						
Amplitudes, mils	1.38	1.91	6.09	41.81	16.52	76.33
Peak speed, rpm	(2625)	(2625)	(2450)	(2550)	(2450)	(2550)
Change, %	+1.5	+21.7	-7.5	-11.2	-10.2	-6.9
Case E — Combination (unbal., warp, skew)						
Amplitudes, mils	1.34	1.72	7.24	50.74	19.89	90.19
Peak speed, rpm	(2625)	(2650)	(2500)	(2550)	(2475)	(2550)
Change, %	-1.5	+9.6	+10.0	+7.8	+8.2	+9.9

[a] Specific excitations:

Case A — Flywheel 50 oz.-in.; motor core 50 oz.-in.; impeller 636.78 oz.-in.
Case B — $\tau = 0.0058798°$; unbalance same as for Case A.
Case C — $\tau = -0.073048°$; unbalance same as for Case A.
Case D — $\theta_d = 0.025°$; unbalance same as for Case A.
Case E — Combination of Cases A, B, C, and D.

[b] Change (%) from Case A: + indicates increase; - indicates decrease.

speed, which was at 484 rpm. The difference between the peak response speed and the undamped critical speed is due to the bearing damping. Note that the unbalance, flywheel skew, and impeller skew excitations did not excite this critical. The warp and combination amplitudes reached 53.5 mils, while the other cases show only 2.5 mils. The former amplitude is 21.4 times the latter. Here, shaft warp has a very significant effect on rotor response at the first critical speed.

The second peak response speed occurs at 2075 rpm for all excitations considered. This peak corresponds to exciting the second undamped critical speed (2132 rpm). The most significant differences at the peak resulted from impeller skew and the combination, with increases of 16% from the unbalance case. Flywheel skew caused only a 4% decrease from the unbalance case, and angular warp caused only a 4% increase. Thus, disk skew (in this case, impeller skew) is the significant factor at the second rotor critical speed.

The third peak response speed occurs at 2550 rpm for all five excitation cases. The corresponding undamped critical speed is 3012 rpm. For this rotor mode, the impeller skew is dominant again, with an increase of 17% from the unbalance case. The combination had a 10% increase, but it contains the impeller skew. The flywheel skew remained essentially the same as the unbalance, and the angular warp caused a decrease of 7%. Therefore, the disk skew (impeller skew) is the significant factor at the third rotor critical speed.

The previous discussion addressed only the response at the pump impeller. However, after carfeul examination of Tables 2 through 4, it is evident that the five excitations have very significant effects at other rotor locations. The conclusions for the first peak remain essentially the same, but at the second peak (Table 3), it is observed that flywheel skew causes a 200% increase over unbalance at the upper motor bearing and flywheel. Furthermore, the angular warp caused increases of 594% at the upper motor bearing, 230% at the flywheel, and 117% at the lower motor bearing. Therefore, the previous conclusion for the second critical speed must be altered. While impeller skew is still a significant factor, the flywheel skew and angular warp effects definitely dominate the rotor response at the second critical speed. Finally, after examining Table 4, for the third peak, the previous conclusion remains basically unchanged. The dominant effect on the overall rotor is impeller skew, with increases between 12 and 19% for all six rotor locations. Note that the flywheel skew does show significant decreases at the upper motion bearing and flywheel (14 and 19%, respectively), and angular warp causes a 22% increase at the flywheel. Hence, disk skew (particularly at the impeller) should be credited as the predominant excitation at the third rotor critical speed. It should be pointed out that for the five excitations used, the phase angles were all arbitrarily selected so that the unbalance, disk skew, and angular warp were in phase. These phase angles do not necessarily represent the worst case, but for the purpose of the comparisons presented, they were sufficient.

In conclusion, for the five cases considered, shaft warp was the dominant factor at the first critical speed, shaft warp and disk skew were dominant at the second critical speed, and disk skew dominated the third critical speed. In the example cases presented in this paper for the industrial water pump, the bearing damping coefficients were reduced by a factor of 20 in order to emphasize the influence of shaft warp and disk skew on the rotor response. The response of the pump with the full bearing characteristics is presented in Ref. (11).

For example, the water lubricated pump bearing has a length of 14 in. and developes a principal damping coefficient of over 7000 lb-sec/in at 1200 RPM. Because of this high damping coefficient, the first critical speed is not readily excited by any form of unbalance. It also should be pointed out that a plain journal bearing in a pressurized environment develops low principal stiffness coefficients and high cross coupling coefficients. Therefore, such a system should also be evaluated to determine its stability characteristics and ability to withstand self-excited fractional frequency whirl.

DISCUSSION AND CONCLUSIONS

This paper has illustrated that disk skew and shaft warp excitations can significantly alter the synchronous rotor response due to unbalance mass excitation alone. This is particularly true when the rotor passes through several critical speeds. To illustrate the importance of these effects on an industrial machine, the governing transfer matrix equations were applied to a large industrial water pump, in which the bearing damping in the three bearings was reduced by a factor of 20 from the original values to excite the first three critical speeds. For this rotor, it was demonstrated that shaft warp was the dominant factor at the rotor first critical speed. Both shaft warp and disk skew had significant effects at the second critical speed. Finally, at the third critical speed, disk skew was the primary influence. Note that for all three critical speeds, the predominant excitation was not unbalance. For this reason, a synchronous rotor response analysis that only considers unbalance excitation could be greatly in error if the actual machine being analyzed has skewed disks and a warped shaft (including coupling misalignment). This error is particularly significant at the rotor critical speeds, which in many machines are excited without reducing the bearing damping. Due to the limitations of manufacturing tolerances, these excitations will always exist to some degree, and their influence must be assessed.

There are many examples of turborotors that do not have the high fluid film bearing damping characteristics as seen in the motor-water pump. For example, aircraft gas turbine engines typically have rolling element bearings. Even with damper supports behind the rolling element bearings, these gas turbine engines usually exhibit much smaller damping characteristics in comparison to industrial rotors on fluid film bearings.

Under these circumstances, the effects of shaft bow and disk skew can be of considerable importance, particularly with overhung power turbines. Another consideration in two spool gas turbines that cycle over a speed range is the possibility of creating thermal bows which can cause shaft warpage and disk skewing. This can result in the transmission of high bearing loads and a corresponding reduction in bearing life.

Another industrial example where the influence of shaft bow and disc skew is of importance is with a double overhung turboexpander. In this type of configuration, one end of the machine has an overhung turbine or expander stage and the other end has an overhung compressor wheel. It is quite possible to bow this type of rotor by thermal gradients, improper shrink fits, or high unbalance loading. If the shaft is bowed, then the wheels also become skewed to the bearing line of centers. The theoretical analysis and actual experience with such a system has shown that it is impossible to perform a satisfactory two plane field balance on the rotor to completely balance the machine at all speeds.

ACKNOWLEDGEMENTS

The authors would like to acknowledge the Babcock and Wilcox Company in Lynchburg, Virginia for their support of the Masters Thesis Research upon which this paper is based. Mr. Salamone, presently with Allis-Chalmers Corporation, was previously employed at Babcock and Wilcox when he completed his thesis work as a graduate student in Applied Mechanics under Dr. Gunter, from the University of Virginia.

Individual acknowledgements are in order for Mr. Harvey D. Ferris, Mr. Robert K. Kennedy, and Mrs. Barbara Eanes of the Babcock and Wilcox Company for their support and cooperation during the preparation of the thesis.

REFERENCES

1 Lund, J. W. and Orcutt, F. K., "Calculations and Experiments on the Unbalance Response of a Flexible Rotor," J. Engineering for Industry, November 1967.

2 Kawamo, K., Matsukura, Y., and Inoue, T., "Analysis of Lateral Vibration Characteristics of Rotating Shafts with Flexible and Axi-Asymmetric Bearings," 1975 Joint JSME-ASME Applied Mechanics Western Conference (1975).

3 Kirk, R. G. and Gunter, E. J., "The Effect of Support Flexibility and Damping on the Synchronous Response of a Single-Mass Flexible Rotor," Journal of Engineering for Industry, ASME Trans. 94:1, Series B, pp. 221-232, February 1972.

4 Wolfe, W. A. and Wong, P. Y., "On the Transfer Matrix for Rotor Dynamics," Manuscript No. 72-CSME-37, EIC Accession No. 1320, July 3, 1974.

5 Barrett, L. E., Gunter, E. J., Allaire, P. E., "Optimum Bearing and Support Damping for Unbalance Response and Stability of Rotating Machinery," J. Engineering for Power, December 1976.

6 Koenig, E. C., "Analysis for Calculating Lateral Vibration Characteristics of Rotating Systems with any Number of Flexible Supports, Part 1 - The Method of Analysis," J. Appl. Math., December 1961.

7 Nicholas, J. C., Gunter, E. J., and Allaire, P. E., "Effect of Residual Shaft Bow on Unbalance Response and Balancing of a Single Mass Flexible Rotor," ASME Trans., Journal of Engineering for Power, Vol. 98, Series A, No. 2, April 1976, pp. 171-189.

8 Yamamoto, T., "On the Critical Speeds of a Shaft," Memiors of the Faculty of Engineering, Nagoya University, Japan, November 1954.

9 Benson, R. C., Dynamic Response of an Overhung, Unbalance Skewed Rotor in Fluid Film Bearings, M.S. Thesis, University of Virginia, August 17, 1974.

10 Kikuchi, K., "Analysis of Unbalance Vibration of Rotating Shaft System with Many Bearings and Disks," JSME Bulletin, June 16, 1969.

11 Salamone, D. J., Synchronous Unbalance Response of a Multimass Flexible Rotor Considering Shaft Warp and Disk Skew, M.S. Thesis, University of Virginia, May 1977.

APPENDIX

The state vector at the right end of the i-th mass station can be expressed in terms of the state vector at the left end of the mass station by means of the point transfer matrix as follows:

$$\begin{Bmatrix} x \\ \theta_x \\ M_x \\ V_x \\ y \\ \theta_y \\ M_y \\ V_y \\ 1 \end{Bmatrix}_i = \left[\begin{array}{cccc:cccc:c} 1 & 0 & 0 & 0 & 0 & 0 & 0 & 0 & 0 \\ 0 & 1 & 0 & 0 & 0 & 0 & 0 & 0 & 0 \\ 0 & -\omega^2 I_T & 1 & 0 & 0 & j\omega^2 I_P & 0 & 0 & \Delta M_x \\ m_s\omega^2 - Z_{bxx} & 0 & 0 & 1 & -Z_{bxy} & 0 & 0 & 0 & \Delta V_x \\ \hdashline 0 & 0 & 0 & 0 & 1 & 0 & 0 & 0 & 0 \\ 0 & 0 & 0 & 0 & 0 & 1 & 0 & 0 & 0 \\ 0 & -j\omega^2 I_P & 0 & 0 & 0 & -\omega^2 I_T & 1 & 0 & \Delta M_y \\ -Z_{byx} & 0 & 0 & 0 & m_s\omega^2 - Z_{byy} & 0 & 0 & 1 & \Delta V_y \\ \hdashline 0 & 0 & 0 & 0 & 0 & 0 & 0 & 0 & 1 \end{array}\right] \begin{Bmatrix} x \\ \theta_x \\ M_x \\ V_x \\ y \\ \theta_y \\ M_y \\ V_y \\ 1 \end{Bmatrix}_i' \qquad (22)$$

where

$\Delta V_x = \omega^2(U_x + jU_y) = \omega^2 U$ = the unbalance term in the x-z plane

$\Delta V_y = -j\omega^2(U_x + jU_y) = -j\omega^2 U$ = the unbalance term in the y-z plane

$\Delta M_x = (I_P - I_T)\omega^2(\tau_x + j\tau_y)$

$= (I_P - I_T)\omega^2\tau$ = the skewed disk gyroscopic term in the x-z plane

$\Delta M_y = (I_P - I_T)\omega^2(\tau_y - j\tau_x)$

$= -j(I_P - I_T)\omega^2\tau$ = the skewed disk gyroscopic term in the y-z plane

$\Delta w_x = \Delta x + j\Delta y$

$\Delta s_x = \Delta\theta_x + j\Delta\theta_y$

$\Delta w_y = \Delta y - j\Delta x$

$\Delta s_y = \Delta\theta_y - j\Delta\theta_x$

$\Delta x = x_{d,i} - x_{d,i-1} - \theta_{x,d,i-1}\ell_i$

$\Delta y = y_{d,i} - y_{d,i-1} - \theta_{y,d,i-1}\ell_i$

$\Delta\theta_x = \theta_{x,d,i} - \theta_{x,d,i-1}$

$\Delta\theta_y = \theta_{y,d,i} - \theta_{y,d,i-1}$

The bearing complex terms are as follows:

1. For a rigid pedestal —

$$Z_{bxx} = S_{xx}$$

$$Z_{bxy} = S_{xy}$$

$$Z_{byx} = S_{yx}$$

$$Z_{byy} = S_{yy}$$

2. For a flexible pedestal —

$$Z_{bxx} = S_{xx}(1 - A_{11}) - S_{xy}A_{21}$$

$$Z_{bxy} = S_{xy}(1 - A_{22}) - S_{xx}A_{12}$$

$$Z_{byx} = S_{yx}(1 - A_{11}) - S_{yy}A_{21}$$

$$Z_{byy} = S_{yy}(1 - A_{22}) - S_{yx}A_{12}$$

where

$$S_{xx} = k_{xx} + j\omega c_{xx}$$

$$S_{xy} = k_{xy} + j\omega c_{xy}$$

$$S_{yx} = k_{yx} + j\omega c_{yx}$$

$$S_{yy} = k_{yy} + j\omega c_{yy}$$

$$A_{11} = \frac{BS_{xx} - S_{xy}S_{yx}}{Q3}$$

$$A_{12} = \frac{BS_{xy} - S_{xy}S_{yy}}{Q3}$$

$$A_{21} = \frac{-S_{yx}S_{xx} + AS_{yx}}{Q3}$$

$$A_{22} = \frac{-S_{yx}S_{xy} + AS_{yy}}{Q3}$$

$$Q3 = AB - S_{xy}S_{yx}$$

$$A = S_{xx} + S_{px} - m_p\omega^2$$

$$B = S_{yy} + S_{py} - m_p\omega^2$$

$$S_{px} = k_{px} + j\omega c_{px}$$

$$S_{py} = k_{py} + j\omega c_{py}$$

Symbols Used on Combined Point and Field Matrix

$$\gamma = m_s\omega^2 - Z_{bxx}$$

$$\lambda = Z_{bxy}$$

$$\eta = Z_{byx}$$

$$\alpha = m_s\omega^2 - Z_{byy}$$

The bearing complex terms are as follows:

For a rigid pedestal —

$$Z_{bxx} = S_{xx}$$

$$Z_{bxy} = S_{xy}$$

$$Z_{byx} = S_{yx}$$

$$Z_{byy} = S_{yy}$$

For a flexible pedestal —

$$Z_{bxx} = S_{xx}(1 - A_{11}) - S_{xy}A_{21}$$

$$Z_{bxy} = S_{xy}(1 - A_{22}) - S_{xx}A_{12}$$

$$Z_{byx} = S_{yx}(1 - A_{11}) - S_{yy}A_{21}$$

$$Z_{byy} = S_{yy}(1 - A_{22}) - S_{yx}A_{12}$$

where

$$S_{xx} = k_{xx} + j\omega c_{xx}$$

$$S_{xy} = k_{xy} + j\omega c_{xy}$$

$$S_{yx} = k_{yx} + j\omega c_{yx}$$

$$S_{yy} = k_{yy} + j\omega c_{yy}$$

$$A_{11} = \frac{BS_{xx} - S_{xy}S_{yx}}{Q3}$$

$$A_{12} = \frac{BS_{xy} - S_{xy}S_{yy}}{Q3}$$

$$A_{21} = \frac{-S_{yx}S_{xx} + AS_{yx}}{Q3}$$

Figure 1 Typical (i-th) Bearing Station Arrangement in y-z Plane With Pedestal Flexibility (Neglecting Rotational Stiffness and Damping Effects)

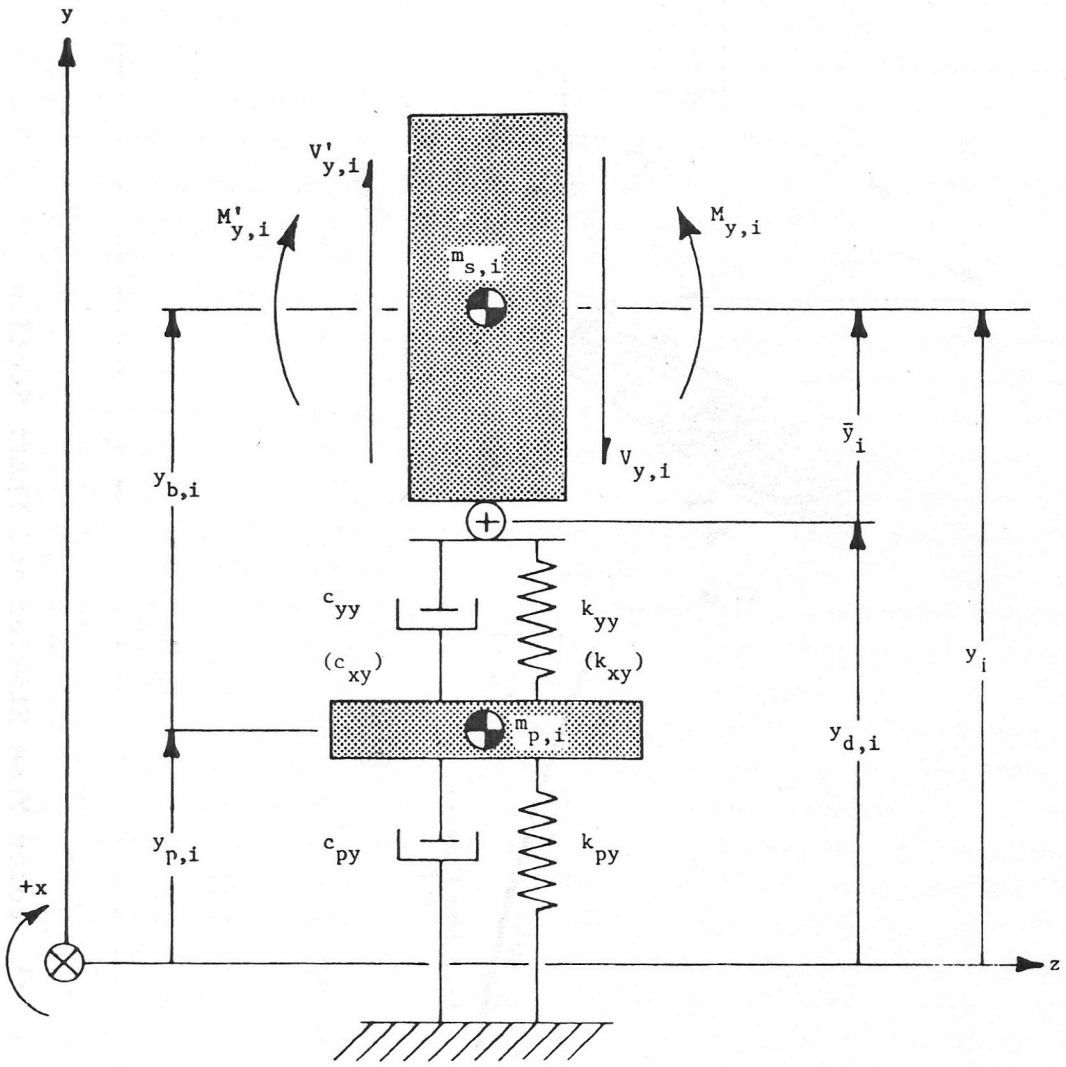

Variable Relationships:

$y_i = y_{p,i} + y_{b,i}$ (Absolute y-displacement of mass station)

$\bar{y}_i = y_i - y_{d,i}$ (Elastic y-displacement of mass station)

where

$y_{p,i}$ = absolute y-displacement of pedestal

$y_{b,i}$ = relative y-displacement of bearing

$y_{d,i}$ = absolute y-distortion deflection (warp) of shaft

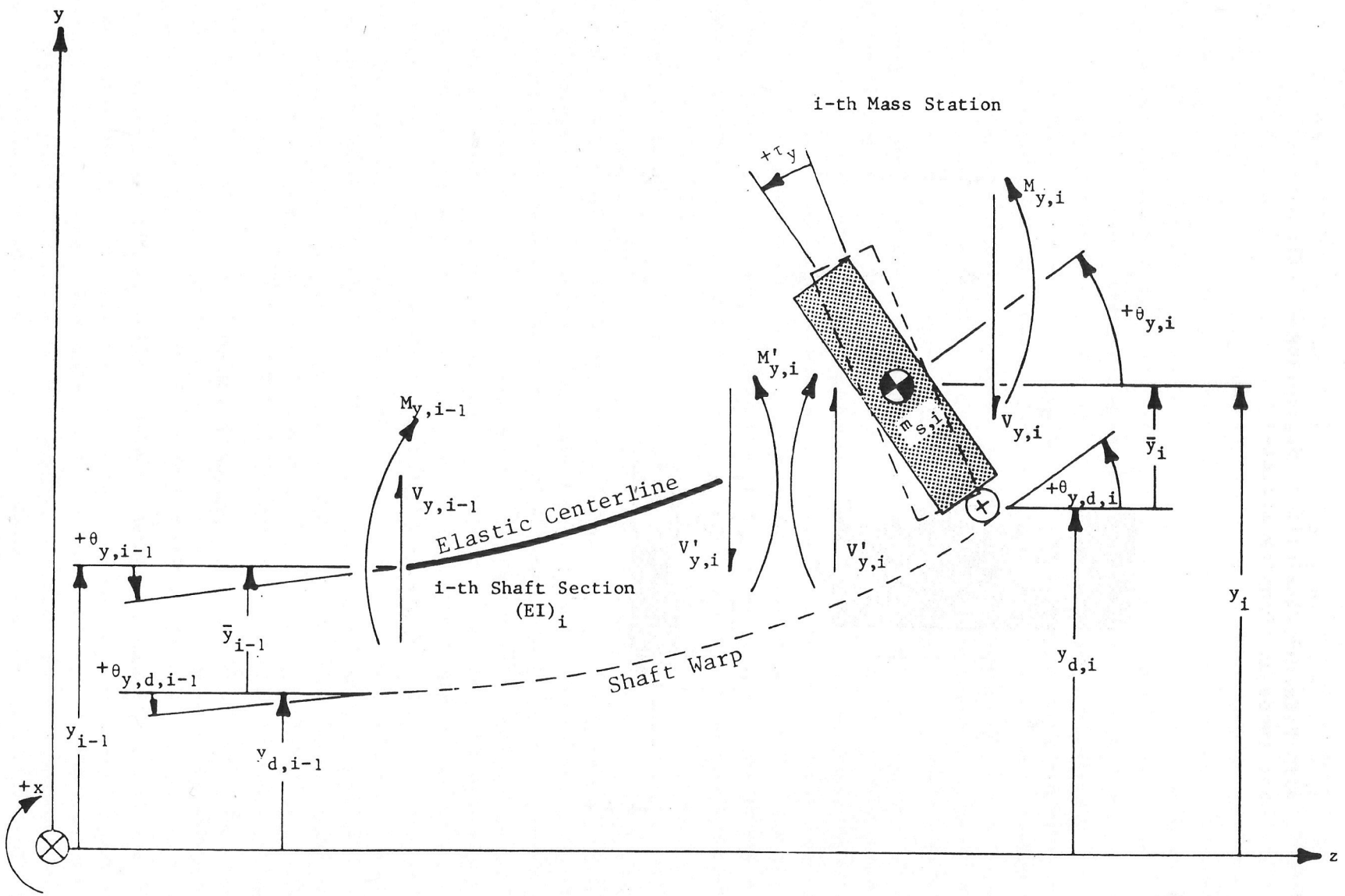

Figure 2 Typical (i-th) Rotor Mass Station and Shaft Section Arrangement in y-z Plane (Note Assumed Sign Convention)

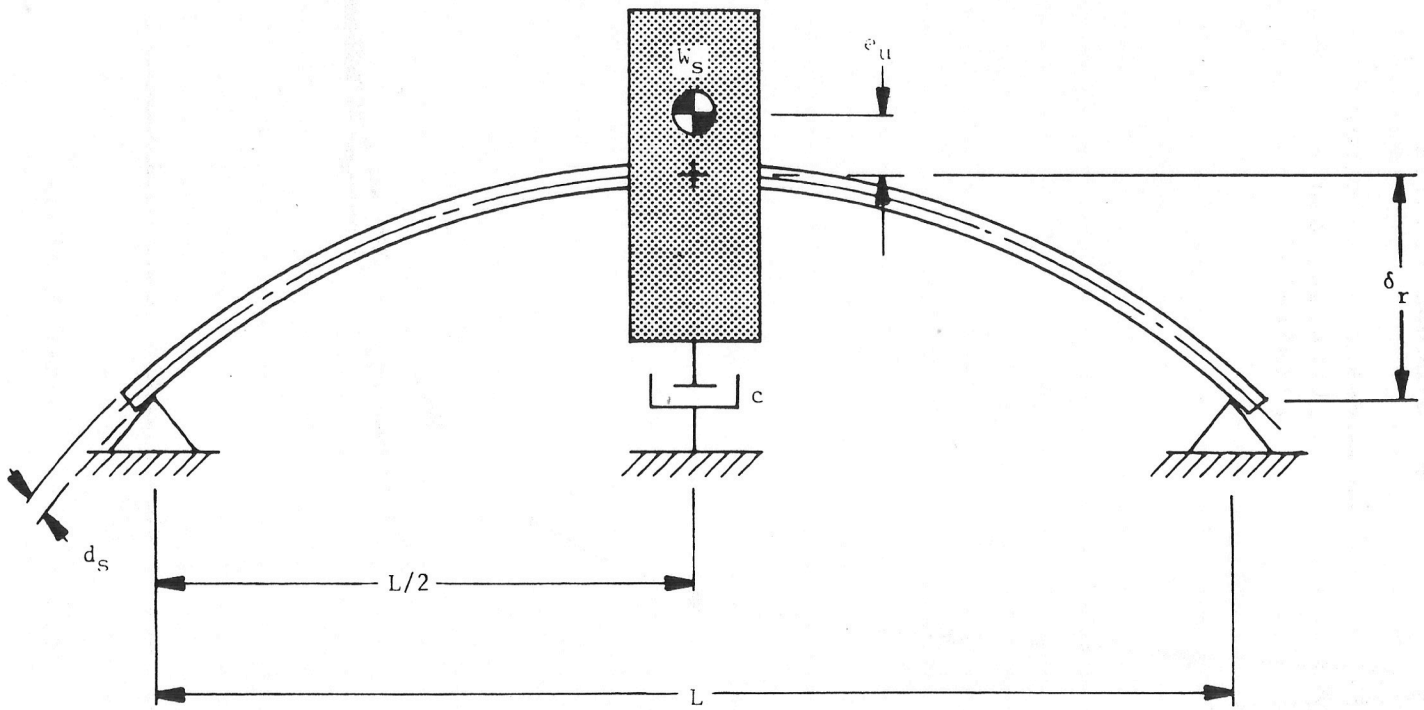

ROTOR MODEL PARAMETERS

L = 50.0 in.	e_u = 0.25 mil	Case I
d_s = 4.0 in.	U_x = 0.3556 oz.-in.	c = 182.57 lbf-s/in. (ζ = 0.5)*
δ_r = 0.125 mil ($\bar{\delta}_r$ = 0.5)*	W_s = 88.9 lbf	Case II
		c = 36.51 lbf-s/in. (ζ = 0.1)*

*Non-dimensional quantity (see reference [6]).

Figure 3 Unbalanced Single Mass Rotor on Rigid Bearings With Warped Shaft and Absolute Damping at Rotor Center

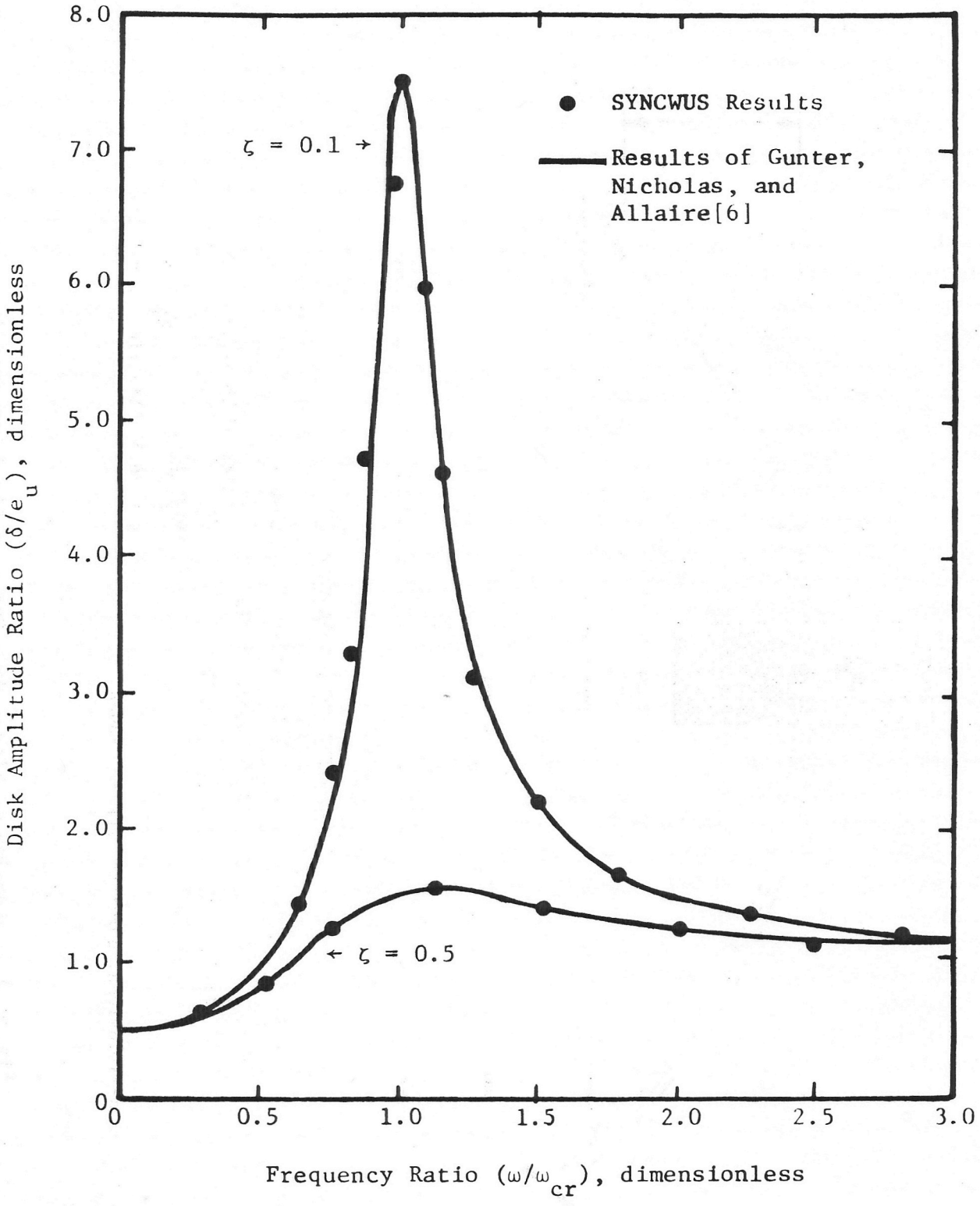

Figure 4 Comparison Between SYNCWUS and Gunter, Nicholas, and Allaire[6] for Disk Amplitude Ratio Vs Frequency Ratio

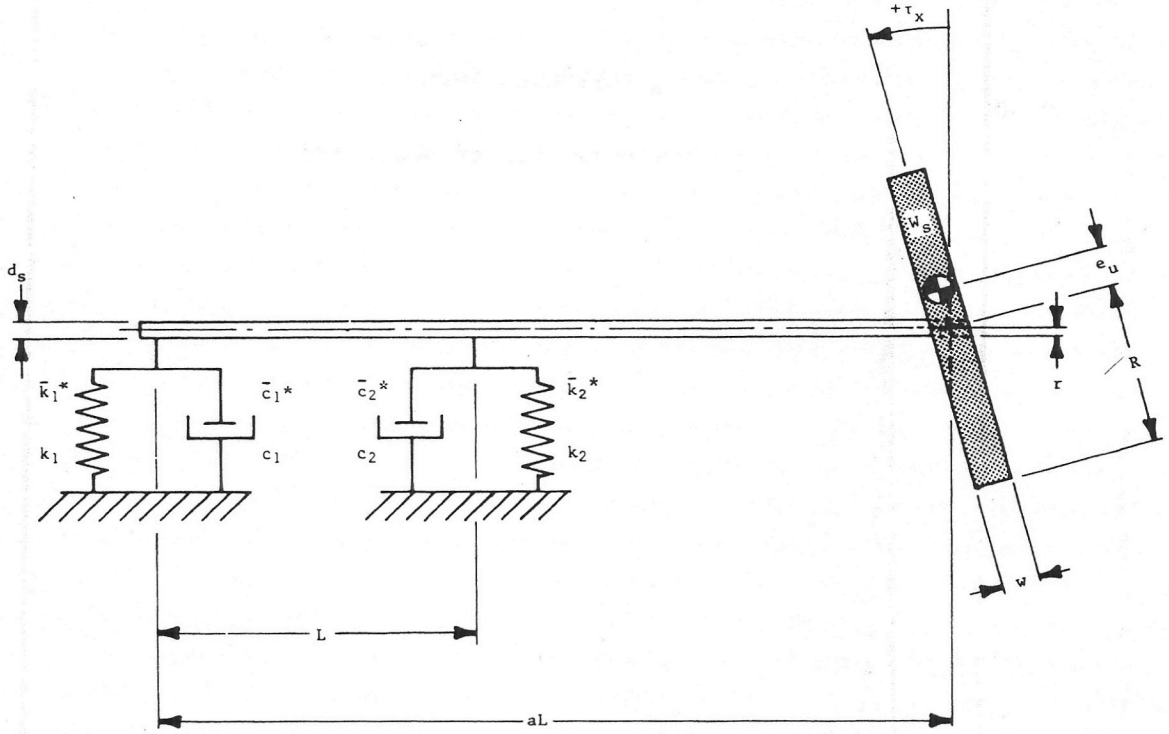

ROTOR MODEL PARAMETERS

L = 101.98 in.	R = 20.0 in.	I_P = 146,461.95 lbf-in.^{2} } [($\bar{I}_P - \bar{I}_T$) = 0.01]*
aL = 135.97 in.	r = 4.0 in.	I_T = 73,231.04 lbf-in.^{2} }
d_s = 4.0 in.	w = 2.0 in.	$k_1 = k_2$ = 7197.9 lbf/in. ($\bar{k}_1 = \bar{k}_2$ = 1.0)*
W_s = 704.14 lbf	e_u = 10 mils	$c_1 = c_2$ = 28.64 lbf-s/in. ($\bar{c}_1 = \bar{c}_2$ = 0.25)*
τ_x = -0.0674°	U_x = 112.66 oz.-in.	

Figure 5 Unbalanced Single Mass Rotor With Overhung Skewed Disk on Flexible Damped Bearings

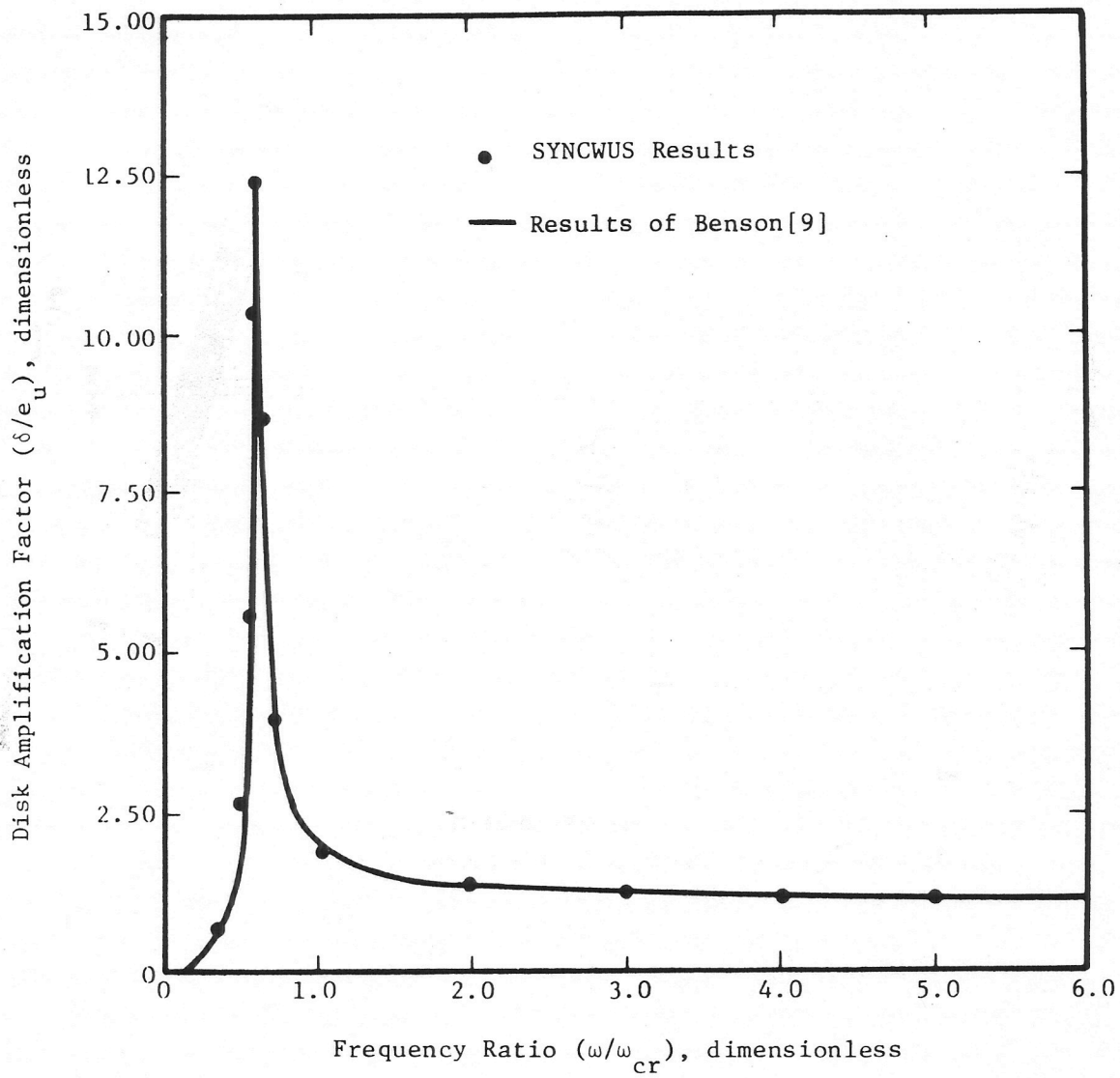

Figure 6 Comparison Between SYNCWUS and Benson[9] for Disk Amplification Factor Vs Frequency Ratio

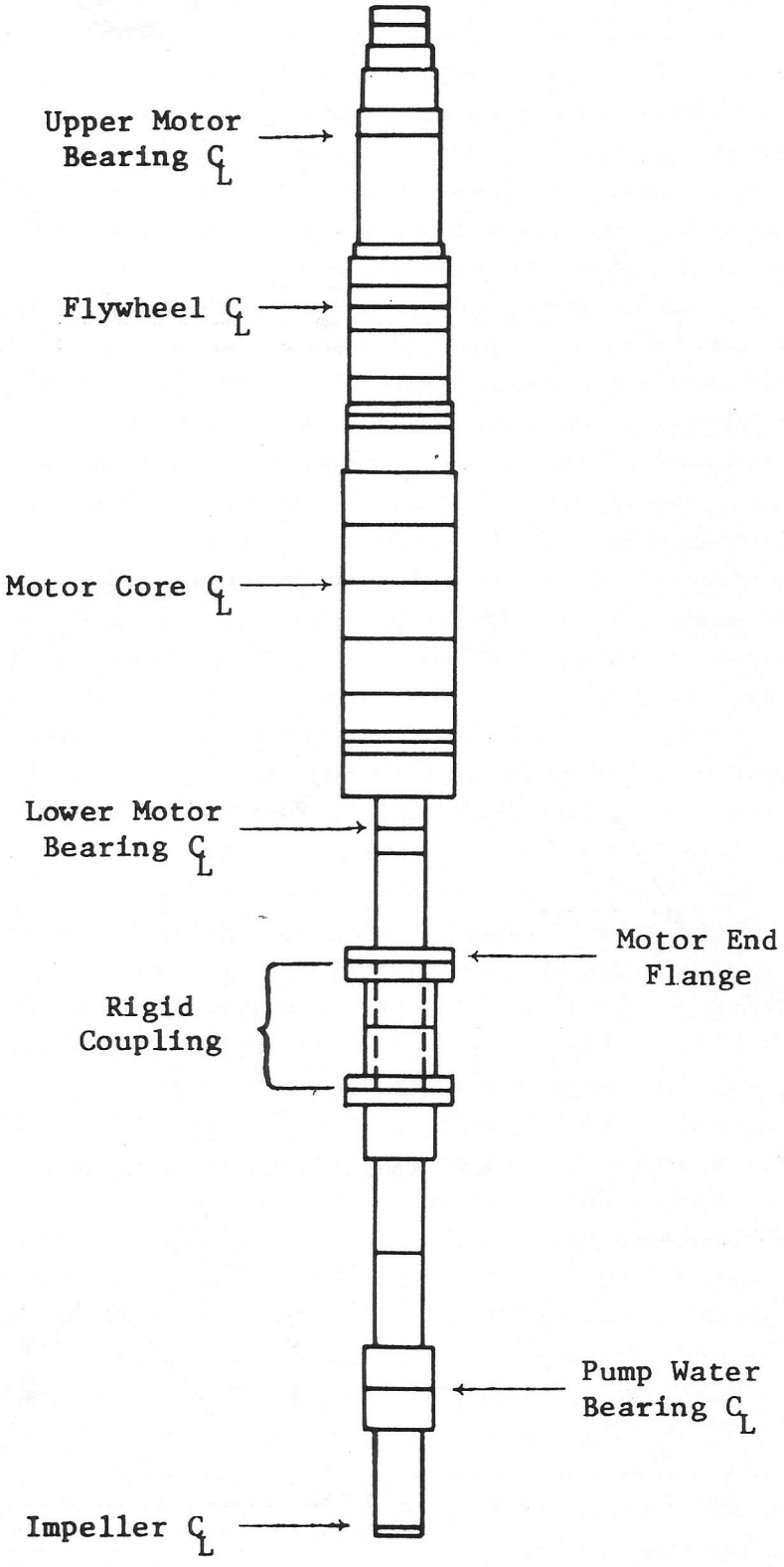

Figure 7 Shaft Cross Section for Large Centrifugal Pump/Motor System

Figure 8 Mode Shape at First Critical Speed

N1 = 483.5 rpm

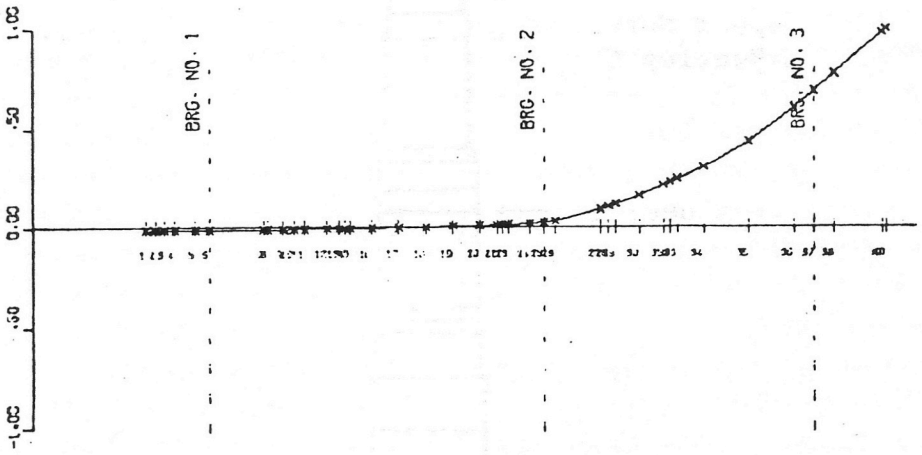

Figure 9 Mode Shape at Second Critical Speed

N2 = 2131.8 rpm

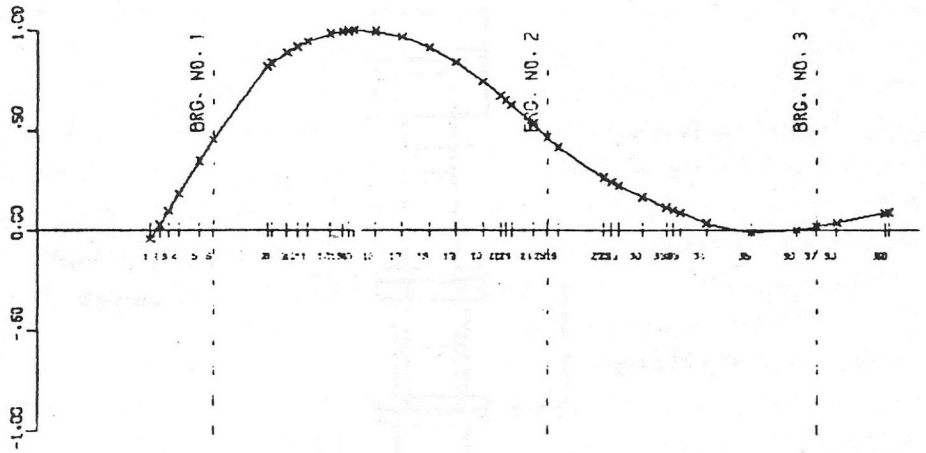

Figure 10 Mode Shape at Third Critical Speed

N3 = 3011.9 rpm

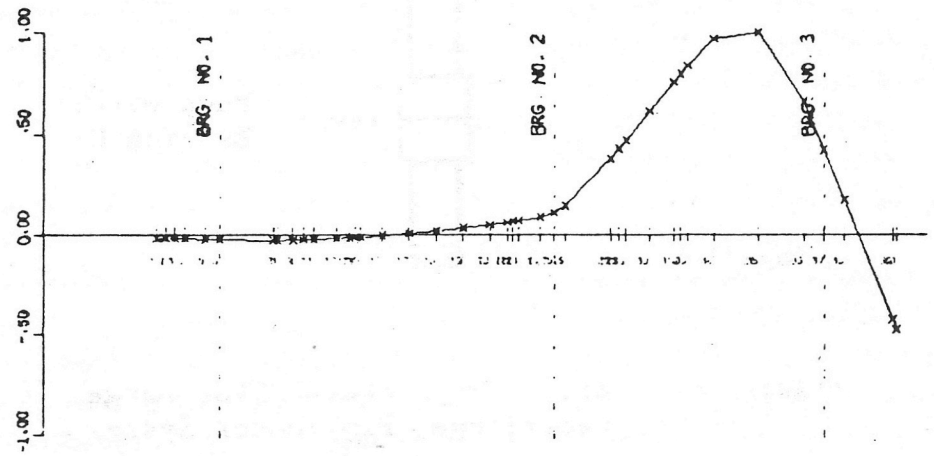

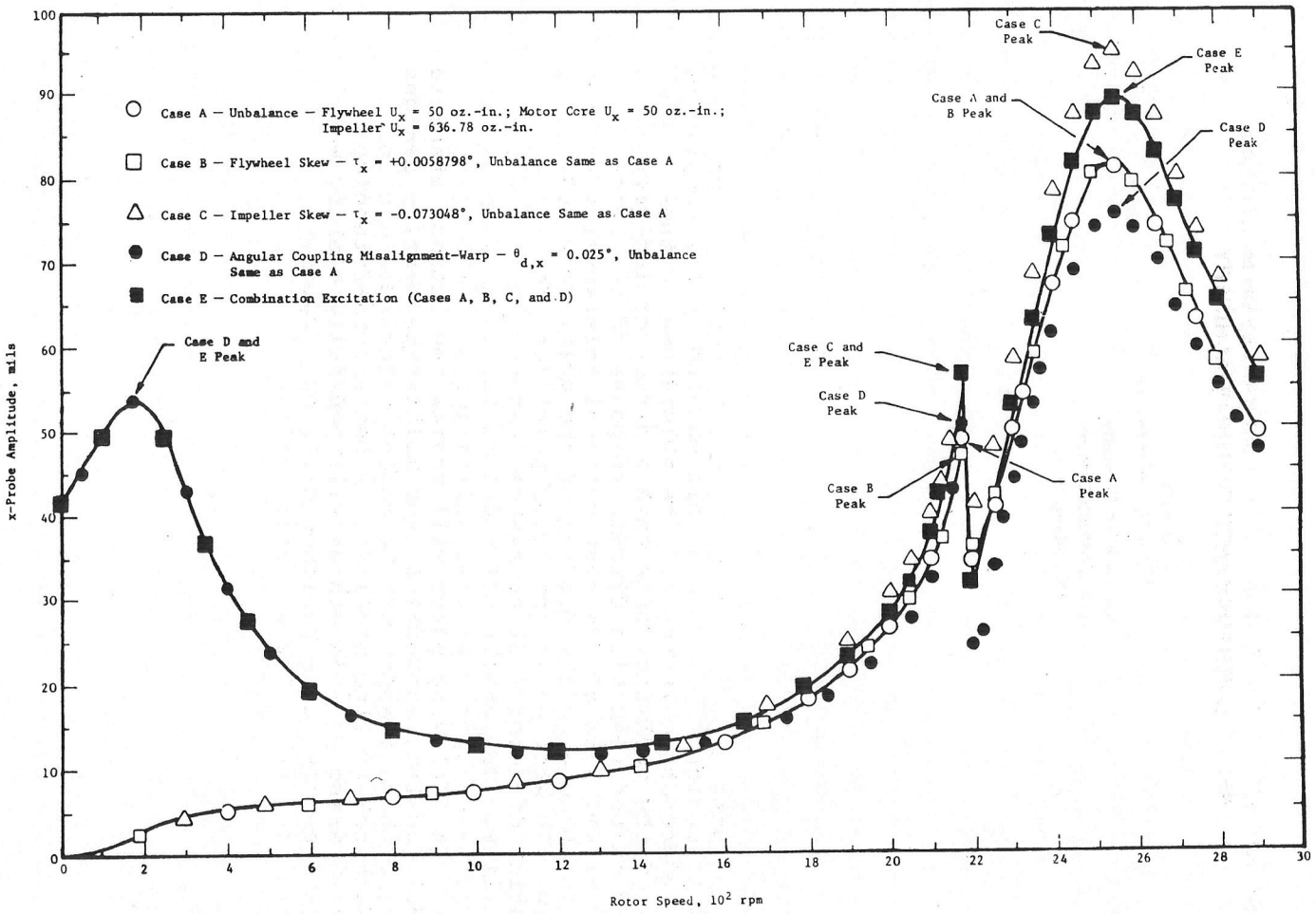

Figure 11 Impeller Amplitudes Vs Rotor Speed (Damping Reduced to 1/20 of Original)